

# A Concurrent Skeleton-based Approach for the Characterization of Wood Fibers with Sub-pixel Precision For Fiber Board Production

Benjamin Seppke<sup>1</sup>, Christian Bähnsch<sup>1</sup>,  
Jan Benthien<sup>2</sup>, Sabrina Heldner<sup>2</sup>, and Martin Ohlmeyer<sup>2</sup>

<sup>1</sup> University of Hamburg, MIN Faculty, Dept. of Informatics, Cognitive Systems  
Laboratory, Vogt-Kölln-Str. 30, 22527 Hamburg, Germany  
{seppke, baehnsch}@informatik.uni-hamburg.de

<sup>2</sup> Johann Heinrich von Thünen Institute, Institute of Wood Research,  
Leuschnerstraße 91, 21031 Hamburg, Germany  
{jan.benthien, sabrina.heldner, martin.ohlmeyer}@ti.bund.de

**Abstract.** The automatic derivation of fiber properties by means of mass data (image) analysis is a current and interesting research area. Skeleton-based approaches have already proven to be adequate in paper pulp quality control [1–3]. However, the derivation for thermo mechanical pulp (TMP) used for the production of medium dense fiberboards (MDF) is, due to the wide range of fiber lengths and fiber morphology, far more challenging. Currently, trained experts are performing the quality assessment visually and haptically on small samples. Since this cannot replace an objective measurement, we propose a fast skeleton-based approach, which is able to derive a variety of fiber characteristics at sub-pixel precision from images of fibers. The algorithm is supposed to work automatically under a laboratory environment for fiber samples, and makes use of concurrency to reduce the processing time and the memory needed. In practice, one measurement cycle is based on approx. 1700 single images with usually more than 1,000,000 automatically measured fibers. Comparisons of the automatically measured fibers with manual microscopic measurements yield in a high reliability and quality of the results.

## 1 Introduction

With a worldwide production of 70 million m<sup>3</sup> in 2010 [4], medium-density fiberboard (MDF) is one of the most important wood-based panels in the market. Manufacturing MDF, wood chips are defibrated into thermo mechanical pulp (TMP), the fibers are glued up with a thermoset resin, and finally continuously hot-pressed into flat panels. In respect to panel properties, fiber board is applied for furniture production, as core material for laminate flooring, as construction or insulation plate, and a variety of other applications. MDF properties are influenced by the fiber quality used, whereby fiber quality is determined by the process parameters applied.

Despite the importance of fiber quality for MDF production, its evaluation is still just done on a low technical level as a worldwide survey of MDF plants [5] showed recently. The overall majority of fiber quality control is yet performed by skilled personnel (haptical and visual), followed by the application of various sieving methods and optical measuring systems with obviously limited capabilities. Based on this initial situation, an alternative image-based fiber analysis system was being developed by the Thünen Institute of Wood Research (Hamburg, Germany); Hamburg University (Hamburg, Germany), in particular Department of Wood Science and The Cognitive Systems Laboratory (KOGS); and Fagus-GreCon Greten GmbH & Co. KG (GreCon) (Alfeld, Germany) in 2009. As a result of the conducted research projects, and on basis of the algorithms presented herein, an offline fiber characterization system has proved to work stable in two industrial trials, each of several months duration [6].

It is the intention of this paper to present a skeleton based image processing approach, which has been developed for the fiber analysis system in order to achieve both, a high computational efficiency and the maximum precision when measuring the fibers optically (cf. [2]). Skeletonization algorithms have their origins in the 1970s, where first pixel-based algorithms have been described by [7, 8]. Since then, many different algorithms have been developed and enhanced by means of morphological image processing ([9–11]). For many applications, the pixel precision of most algorithms may not be sufficient to achieve reliable measurement results. However, only comparably few sub-pixel skeletonization methods exist and are often computationally expensive [10, 12]. Due to wide range of fiber sizes and the varying fiber morphology, a new algorithm for the automatic measurement of pre-separated fibers will be described herein. To achieve the largest possible sample set of fibers, high-resolution images need to be analyzed. While the high resolution is able to monitor even smaller (dust) fibers, these fibers are quite above the minimal size required by the sampling theorem (see [13]). To avoid measurement errors, a sub-pixel approach is proposed. To save both, memory and computation time, the algorithm is designed to be executed concurrently, which allows a faster processing on modern CPUs.

## 2 Mechanical fiber separation and image acquisition

The technical set-up of the measuring device hardware component can be roughly partitioned into three sections: (a) mechanical fiber separation, (b) image acquisition, and (c) cleaning (Fig. 1). The mechanical fiber separation is arranged by means of specially tuned airflows, and completes when the fibers land as a fine scattered film on the continuously rotating glass plate, which can be considered as the objective plate. Passing the photo unit, a large subsample of the fibers on the objective plate is imaged with an industrial high-resolution grayscale camera (GE4000, Allied Vision Technologies GmbH, Stadtroda, Germany). Each image corresponds to a size of  $93 \times 62$  mm on the objective plate, with a reference size of  $23.2 \mu\text{m}$  per pixel.

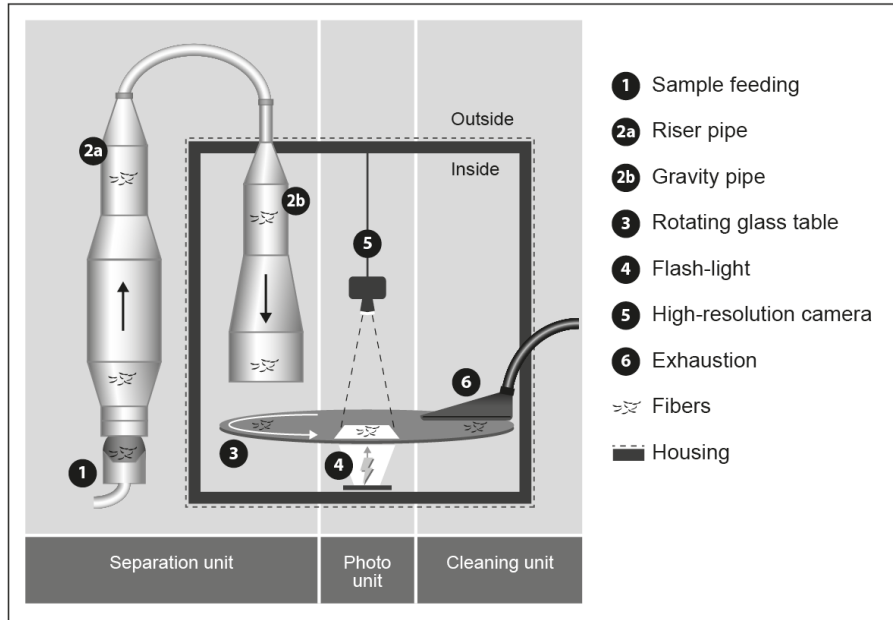


Fig. 1: Structural diagram of the experimental setup. The fibers are pre-separated (left) before they fall on the objective plate and are being imaged (center). After acquisition, the fibers are removed from the plate by vacuum. (modified Fig. from [5]).

The image recording is arranged with a frequency of approximately 82 photographs per minute, resulting in approx. 1700 photographs per measuring cycle. Each measurement cycle is divided into three sub cycles, where new fibers are inserted into the separation unit's container. This is necessary, since the separation has a capacity of about 0.5g. Usually, fiber samples of millions of MDF fibers correspond to a weight of approx. 1.5g. A complete cycle is currently performed in less than 30 minutes. This includes the time, which is necessary for stopping the machine, refilling fibers, restarting the machine, and resuming the measurements. The resulting count of fibers depends on the fibers' types and characteristics (Fig. 2).

To achieve the best contrast between fibers and the empty objective plate in each image, the images are taken using an area-flashlight, which is triggered in conjunction with the camera and emits light in the red spectral range. Thus, the fibers are imaged darker than the surrounding (empty) background. After each image acquisition the glass plate is rotated and cleaned up by a vacuum cleaner. Parallel to its acquisition, images are grabbed and a scheduled for concurrent processing by the software algorithm presented in this paper (see Fig. 3).

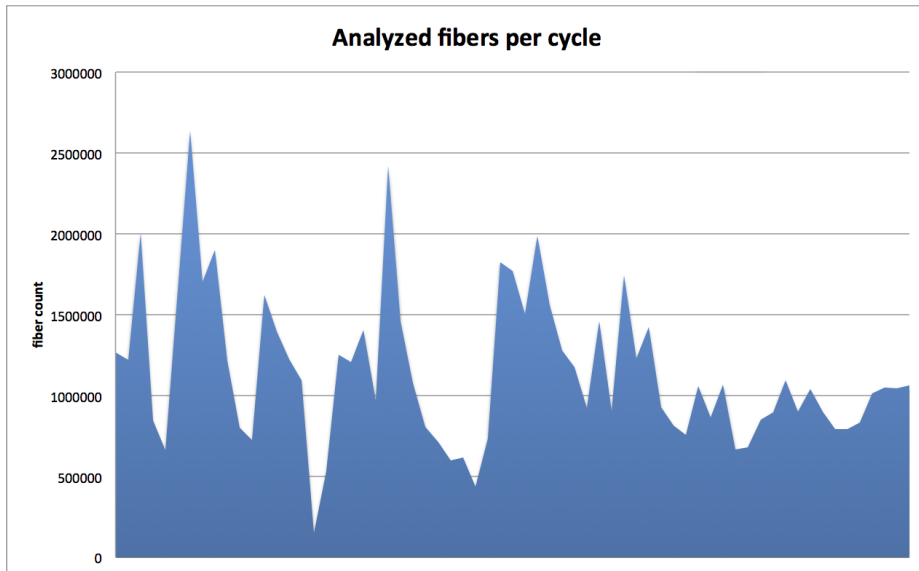


Fig. 2: Count of measured fibers for different sample test cycles with MDF fibers. The count has a range of 150750 – 2637385 fibers, with a mean of 1142550.4 and a standard deviation of 465016.9 fibers.

### 3 Image Processing

The experimental setup directly influences the choice of the applicable image processing methods. The images of the fibers are taken on a transparent (glass) surface, which is backlit using an area flash at each acquisition. Since the fibers on the glass shut off light, they are imaged using darker image intensities when compared to the uncovered objective plate. Additionally, we expect an intensity gradient from the fibers center to the surrounding areas.

#### 3.1 Preprocessing

The camera is grabbing 16bit grey-scale images, thus the first step is to preprocess the images by means of noise reduction and the decision if a pixel of the acquired image is representing a fiber. To estimate a bias or control image, the clean object plate is firstly rotated without fibers applied to calibrate for  $n$  empty images  $C = \{CI_1, \dots, CI_n\}$ .

After this calibration run, the acquired images are aggregated to a mean reference image for the preprocessing during the measurements. Before the decision whether a pixel is covered by a fiber, the current image is (absolutely) subtracted from this reference image:

$$I_p = \|\bar{C} - I_a\|$$

Based on this absolute difference image a user-selected threshold is applied to derive the so-called fiber mask of the image  $I_m$ , which assigns a pixel either to represent a fiber or the (former brighter) background.

$$I_m = \begin{cases} 1 & \text{if } I_p > t_f \\ 0 & \text{else.} \end{cases}$$

The next processing step is the application of a fast union-find labeling algorithm to the mask to detect 4-connected regions of fiber pixels. We use an efficient implementation of the algorithm proposed by Roerdink in [14]. Based on the derived connected components a pre-filtering takes place. a region will be dismissed if its bounding box touches the image boundary as the image function is unreliable at boundaries and fibers may be partially excluded from the acquisition field.

The processing of each region is then performed in a concurrently manner. To allow a correct processing of shive regions, another classification step is introduced for each region. Pixels representing dark and thick areas are classified by using a minimal thickness threshold  $t_{sd}$  and a minimal intensity value  $t_s$  are marked in  $I_s$ . The thickness estimation is based on a distance transform of the fiber mask for each region.

$$I_s = \begin{cases} 1 & \text{if } I_p < t_s \text{ and } dist(I_m) > t_{sd}/2 \\ 0 & \text{else.} \end{cases}$$

In order to compute valid sub-pixel fiber skeletons, each region with an associated shive classification will be smoothed before the next processing step to generate less sub-pixel extrema. The smoothing is carried out by means of a Gaussian smoothing kernel, which standard deviation is determined according to the maximum value of the distance transform of the region. Thus, regions with “thicker” shives are proportionally more smoothed.

### 3.2 Fiber skeleton graph creation

Each connected component may correspond to either a single MDF fiber or an aggregation of different non-isolated fibers. The next step is to determine the structure of the imaged signatures. To speed up this part of the developed algorithm the fiber segmentation is applied to each connected component concurrently using a unique identifier and the mask as well as the image data for the bounding box of the former step. The segmentation of the fibers of each connected component is based on a sub-pixel skeletonization approach proposed by Meine in [15]. This approach determines sub-pixel precise local maxima and saddle points. After the determination, a Runge-Kutta optimization approach is used to trace flow lines from each saddle point to eventually connect it to the closest local maxima. In contrast to Meine, who applied this approach on a gradient image to derive a sub-pixel watershed segmentation of the image, we apply the algorithm on the preprocessed image data.

The resulting directed graph  $G = (V, E)$  will then be used as a definition of the inner structure, the skeleton, of each connected component. Additionally, a geometrical embedding function  $geo : V \rightarrow \mathbb{R}^2$  is defined to map each vertex to a sub-pixel image position. Despite other works on fiber recognition, this accuracy is needed due to the large range of fiber sizes, to ensure the accurate measurement of smallest fibers (cf. [2, 3]).

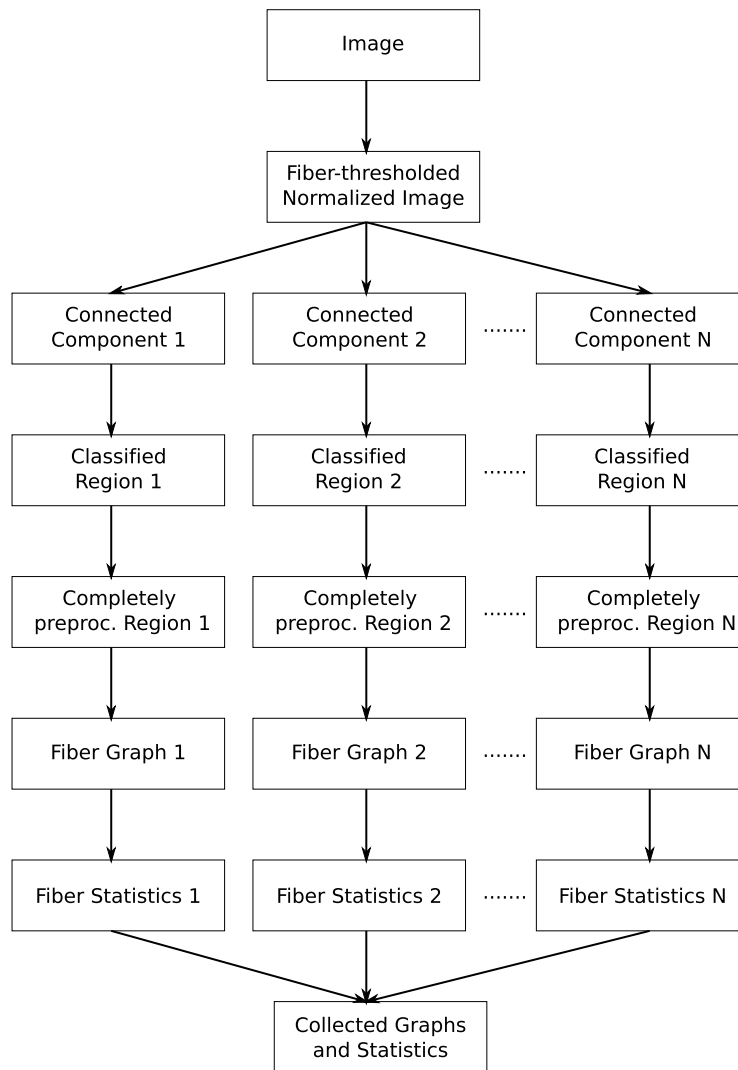


Fig. 3: Algorithmic design. From top to bottom: general execution direction. From left to right: concurrent computing.

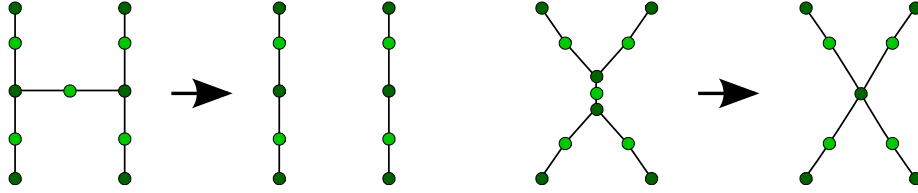


Fig. 4: The resolution of H-configurations. Left: streamer configuration, right: erroneous crossing configuration. From left to right: initial configuration, proposed fix. Light green: saddle points, dark green: (pseudo) maxima.

## 4 Fiber graph processing

After the creation of the graph, the graph is the universal data structure, where all future steps and the measurements will take place. But before the measurement, some graph structures need to be analyzed and eventually be fixed in order to achieve a structural correspondency between the graph and the imaged MDF fibers.

### 4.1 Resolving H-configurations

After the creation, we need to fix the structure of the graph by means of erroneous detected crossing configurations. Since the graph was derived purely by the image itself, some crossings may be degenerated to a H-configuration. Additionally, so-called streamers may also result in such configurations (cf. [15]).

For each saddle vertex  $v$  with exactly two neighbored vertices  $v_1$  and  $v_2$  in  $V$ , let  $geo(v) = (x, y)^T$  and  $geo(v_i) = (x_i, y_i)^T$  denote the geometrical embedding of the nodes.

An H-configuration is defined at vertex  $v$  if and only if each of the vertices  $v_1$  and  $v_2$  have exactly two neighbors different from  $v$ , namely  $v_{11}$ ,  $v_{12}$ ,  $v_{21}$  and  $v_{22}$  and each of these neighbored vertices has a degree of 2 (see Fig. 4). The resolving of such H-configurations is performed using the following algorithm:

1. Compute the angles  $a_i$  between  $v_i$ ,  $v_{i1}$  and  $v_{i2}$  for  $i \in \{1, 2\}$ .
2. If  $a_1 \approx 180^\circ$  and  $a_2 \approx 180^\circ$  and  $I(x_1, y_1) > I(x, y)$  and  $I(x_2, y_2) > I(x, y)$ :  
 Streamer configuration: the vertex  $v$  will be removed from  $V$  and all edges connecting to or from  $v$  in  $E$  will be deleted, too.
3. Else: Compute the angles  $c_{ij}$  between  $v_{1i}$ ,  $v$  and  $v_{2j}$  for  $i, j \in \{1, 2\}$ .
4. If  $\max(c_{ij}) \approx 180^\circ$ :  
 Erroneous crossing configuration: contract the vertices  $v_1$  and  $v_2$  to  $v$ . Thus,  $v_1$  and  $v_2$  will be removed from  $V$ , corresponding edges will be removed, too. Eventually edges from  $v$  to  $v_{11}$ ,  $v_{12}$ ,  $v_{21}$ , and  $v_{22}$  will be inserted into  $E$ .

## 4.2 Adding pseudo-graphs for small connected components

Another consequence of the graph creation algorithm is, that a skeleton can not be derived for all detected regions. Small regions e.g. may not provide any (or only one) local maxima. To cope this, we distinguish between two cases for connected components whose graphs have an empty set of edges:

1. If the size of the connected component is one pixel:  
Add two vertices placed slightly left and right of the detected maxima and connect them to the central maxima vertex.
2. If the size is larger than one pixel:
  - (a) Compute the normalized image moments up to second order:  $m'_{ij}$  with  $i, j \in \{0, 1, 2\}$  and  $i + j \leq 2$ .
  - (b) Derive the center of gravity:  
 $\mathbf{g} = (m'_{10} \ m'_{01})^T$ .
  - (c) Define the covariance matrix  
$$A = \begin{pmatrix} m'_{20} & m'_{11} \\ m'_{11} & m'_{02} \end{pmatrix} - \mathbf{g} \cdot \mathbf{g}^T$$
  - (d) Solve the Eigen system of  $A$ ,  
Let  $\mathbf{ev}_+$  denote the major eigenvector of  $A$ .
  - (e) Clear the current graph.
  - (f) Add two vertices  $v_1$  and  $v_2$  to the graph. Connect them using edges.
  - (g) Set the geometrical embedding as follows:  
 $geo(v_1) = \mathbf{g} - a \cdot \mathbf{ev}_+$  and  
 $geo(v_2) = \mathbf{g} + a \cdot \mathbf{ev}_+$   
where  $a$  is a scaling factor with  $0 < a < 1$ .

After the execution of the above algorithm either a graph or a pseudo-graph is assigned to each connected component of the image.

## 4.3 Resolving crossing fibers

Due to errors in the mechanical separation process or large compounds (shives), the classified pixels of each region may correspond to more than one wood fiber. Thus, based on the skeleton of each region, overlaying fibers need to be splitted before the derivation of fiber statistics.

Instead of a real graph splitting, which would require the addition of new vertices, we extend the graph structure by a special set of edges, which we will refer to as "bypasses". In contrast to the edges, each bypass  $b(v_1, v_2, v_3) \in B$  defines a triple, where  $v_1$  defines the start vertex of the bypass,  $v_2$  the vertex, which is bypassed, and  $v_3$  the target of the bypass. Using this notation, all other graph information is still available and the graph traversal by means of deriving fiber properties can be performed in a clearly defined way.

To determine if there is an bypass, we perform the following analysis steps for each vertex  $v$  with a set of neighbors  $NB = \{w \mid (v, w) \in E\}$  with  $card(NB) = n$  and  $n > 2$ :

1. Create a square matrix of size  $n \times n$ :  $A$
2. For each pair of neighbors  $w_i, w_j$ :  
Determine the angle between  $w_i, v$  and  $w_j$  and store it as  $a_{ij}$  and  $a_{ji}$  in  $A$ .
3. Let  $a_{ij}$  be the  $\max(a)$ , e.g. the angle, which is the closest to  $180^\circ$ .
4. While  $a_{ij} > 180 - \text{ang}_t$ :
  - (a) Create new bypasses  $b(w_i, v, w_j)$  and  $b(w_j, v, w_i)$ .
  - (b) Reset the angles in matrix  $A$ :  $a_{ij} = a_{ji} = 0$
  - (c) Proceed with the next max. angle of  $A$ .

where  $\text{ang}_t$  is an angular valued threshold, which describes an lower angular border for bypass creation. If e.g.  $\text{ang}_t = 40^\circ$ , than only traversals with a deviation of  $40^\circ$  over  $v$  will be considered as bypasses. Since the proposed greedy algorithm runs iteratively on each vertex, multi-crossings may also be resolved by means of the best pairs below the angular threshold  $\text{ang}_t$ .

#### 4.4 Fixing the end vertices of fibers

Due to the generation steps of the graph, the length of a fiber might be underestimated. The reason for this underestimation is the use of local maxima as vertices. The end of the fiber, however, may be pixels beyond the last local maximum found. To solve this problem, we propose to fix these underestimated end vertices. The proposed algorithm works as follows. For each end vertex  $v$  in  $V$ , which has exactly one neighbor  $w$  with  $e(v, w) \in E$ :

1. Let  $\mathbf{a} = \text{geo}(v) - \text{geo}(w)$  be the direction vector from vertex  $w$  to vertex  $v$
2. Normalize the vector  $\mathbf{a}' = \|\mathbf{a}\|$ .
3. Set  $\mathbf{p} = \text{geo}(v)$ .
4. While  $\mathbf{p}$  is inside the connected component:  
Set  $\mathbf{p} = \mathbf{p} - c \cdot \mathbf{a}'$ ,  
where  $c$  is a constant factor with  $0 \leq c \leq 1$ .
5. Add  $x$  as a new vertex to  $V$ .
6. Add the geometrical embedding  $\text{geo}(x) = \mathbf{p}$
7. Connect  $x$  with  $v$ .

After the algorithm, for each former end vertex, another end vertex is introduced and shifted away from the former end vertex until the end of the fiber mask is reached.

#### 4.5 Derivation of fiber characteristics

After the extraction of the fiber skeleton, the fiber characteristics may be derived by means of traversing the graph and collecting information during the traversal. The selection of statistical fiber properties is based on providing a huge variety of basic features (see [3]) and is especially tailored to the needs of the researchers at the Thünen Institute of Wood Research:

- Length [ $\mu\text{m}$ ]  
The length of a fiber is defined as the overall distance between all traversed vertices.
- Width [ $\mu\text{m}$ ] (min., max., mean and std. dev.)  
Since the width of a fiber may vary, it is determined for every visited vertex using a distance transform of the fiber mask. Afterwards, the statistical properties are derived.
- Curvature [ $^\circ$ ] (min., max., mean and std. dev.)  
Since the curvature of a fiber may vary too, it is determined for every visited vertex (except the first and last vertex) by computing the angles between three successive vertices. Afterwards, the statistical properties are derived.
- Intensity (min., max., mean and std. dev.)  
The intensity of a fiber may also vary. Thus it is determined for every visited vertex before the statistical properties are derived.

During the traversal, each visited edge is marked, to ensure that it will only be counted once. Additionally, information about the fiber classification is derived during the traversal. We distinguish between three different kinds of fibers:

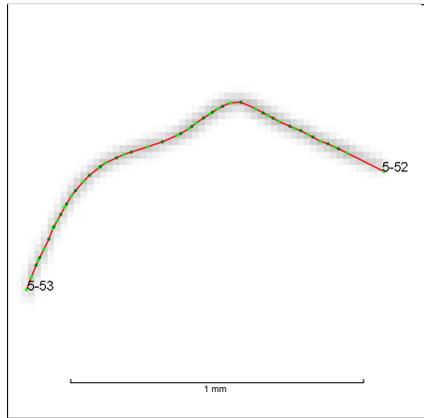
1. Complete fiber  
All of the traversed vertices are located inside image areas classified as "fibers".
2. Touching shive  
All but the first or the last of the traversed vertices are located inside image areas classified as "fibers". The first or the last vertices may however be classified as shives.
3. Shives  
Nearly all vertices (we currently use a threshold of 90%) are located inside image areas, which have been classified as shives.

The threshold is needed due to the extension of end vertices. The result of image analysis is exported in form of CSV-files, further processed by a MATLAB routine, and finally used for the characterization of the analyzed fibers.

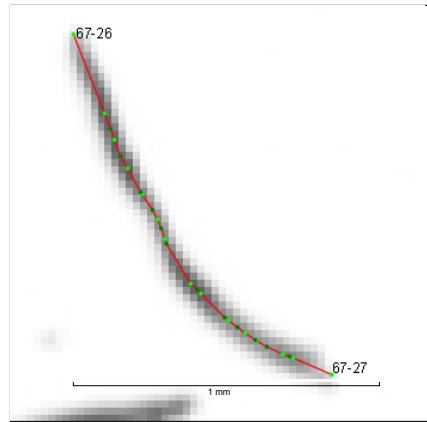
## 5 Results

Before the three-month industrial trial, where the automated offline fiber characterization has proved to work stable, the presented algorithm has been applied to comparative microscopic measurements of the same fiber set. Since the microscopic measurement has to be performed manually and is very time-consuming, the comparison is based on a set of only 400 fibers. These 400 fibers have been manually measured and characterized w.r.t. their lengths and widths.

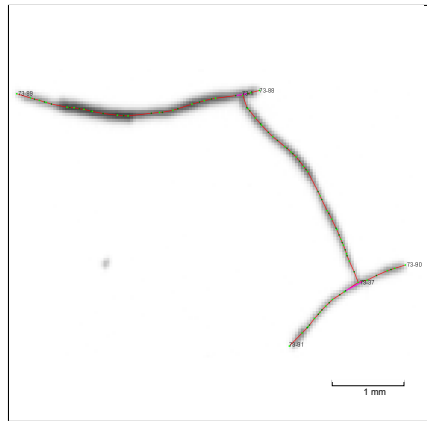
We will now discuss the individual results for a set of 6 fibers. The fibers have been selected to repeat prototype, which differ in lengths and in morphology. Additionally, some of the fibers have not been pre-separated and thus are imaged overlaid onto each other. The sub-images of these fibers are shown in Fig. 5.



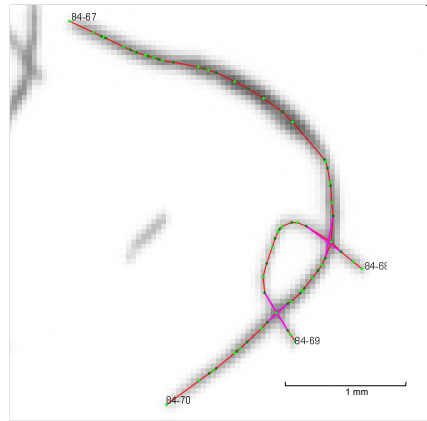
(a) Example 1: single fiber (thin)



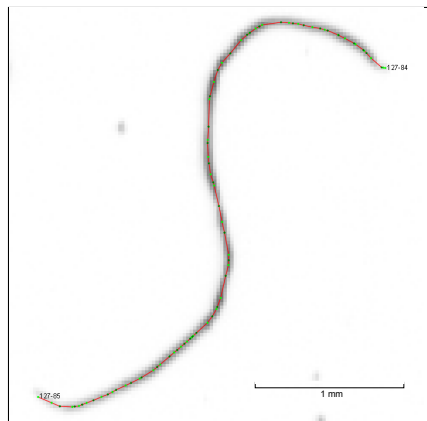
(b) Example 2: single fiber (thick)



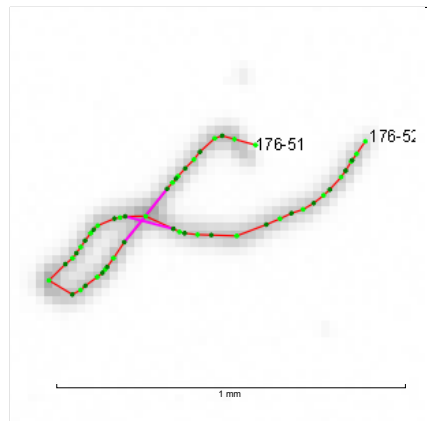
(c) Example 3: touching fibers



(d) Example 4: crossing fibers



(e) Example 5: long fiber



(f) Example 6: self-crossing fiber

Fig. 5: Examples 1-6, extracted from the test set. Note that the examples are not to scale, when compared to with each other. The start and end-nodes of each fiber are uniquely labeled, bypasses are highlighted in magenta.

Table 1: Comparison of computed (automatically derived) and (microscopic manually) measured fiber lengths for the examples of Fig. 5. A deviation of one pixel corresponds to approx. 23  $\mu\text{m}$ .

<b>Example</b>	<b>computed</b> [ $\mu\text{m}$ ]	<b>microscope</b> [ $\mu\text{m}$ ]	<b>deviation</b> [ $\mu\text{m}$ ]
1	1113.93	1115.82	1.88 (0.17 %)
2	996.29	994.66	1.63 (0.16 %)
3	1337.79	1322.90	14.89 (1.11 %)
3	1204.08	1192.57	11.51 (0.96 %)
3	779.79	768.94	10.85 (1.39 %)
4	713.17	739.41	26.24 (3.68 %)
4	1966.21	2019.39	53.18 (2.70 %)
5	3064.32	3114.90	50.58 (1.65 %)
6	1298.97	1329.55	30.58 (2.35 %)

Table 1 shows the individual deviations between automatically derived and microscopic (manually) measured fiber lengths. The results are promising with quantitative deviations of only 0.17% to 3.68%, referring to a range from less than 0.1 up to about 2 pixels w.r.t. the 1600 dpi of the scanned image. Since the microscopic measurements deviate from person to person, this can be considered as a nearly perfect match. This is insofar remarkable as it took several hours for a trained expert to perform the microscopic measurements but only about one second for the algorithm to determine even more fiber characteristics, like the curvature or intensity of a fiber. It should be mentioned, that the width measurements show similar results.

Beside the agreement of single fibers' characteristics, we analyze the overall agreement of all measured and derived fibers. Since some of the measured fibers were not included in the microscopic measurements and vice versa, we decided to compare both values based on each (sorted) fiber subset. The results of the comparison with respect to the fiber length are shown in Fig. 6. The result of this comparison is the overall agreement of microscopic and automated measurements. Moreover, it supports the statistical quality of the automatically derived fiber properties. With a correlation coefficient of approx. 1, we are able to argue and to replace costly and slow microscopic measurements by the method presented herein.

After the quantitative evaluation of the proposed algorithm, it has been implemented in a multi-threaded manner using the VIGRA library (see [16]) for the implementation of the computer vision tasks and the Qt4-Framework to provide a graphical user interface and a framework for concurrent processes (see [17]). The software is connected to the experimental setup by means of a trigger signal of the camera grabber. On each trigger signal it performs the grabbing of images, the calibration, the analysis of the fibers using the algorithm presented herein and the storage of the results by means of comma separated values and scalable vector graphics, which contain the extracted graphs for each acquisition.

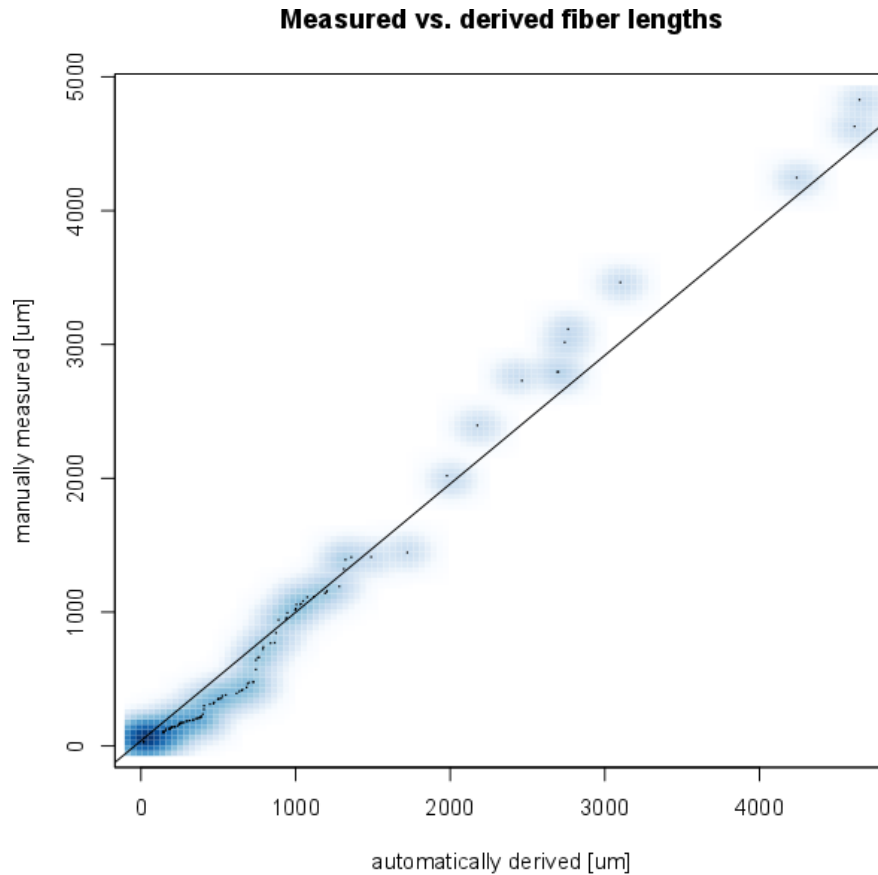


Fig. 6: Scatter plot of the quantitative evaluation for a randomly selected set of 400 fibers. Diagonal: regression line representing a correlation of 1.0. The derived correlation coefficient is: 0.9933823.

## 6 Conclusions

In order to overcome current limitations in TMP fiber quality and MDF process control KOGS, Department of Wood Science, Thünen Institute of Wood Research and GreCon started to develop an inline- and an offline operating fiber analysis system in 2009. Since the inline system operates in three German MDF plants and the offline system has proven to work stable by analyzing millions of fibers in thousands of images in a first industrial trial, it was the intention of this conference contribution to present details of the developed software for fiber characterization using mass image analysis. We have shown that the approach of Meine is, with some modifications, capable for sub-pixel precise skeleton graph derivation, too (cf. [15]).

The algorithmic design is based on the map-reduce design pattern, which allows the algorithm to run in multiple threads/processes, one for each connected component. Since modern CPUs already consist of multiple processing units, we achieve a maximum performance speed up in order of the number of available (threading) cores. However, this speed up is also depending on the number of connected components in the pre-classified image. Besides the innovative (non-liquid) fiber pre-separation, and flow line tracing during image analysis, the software-based separation of cross-laying fibers was one of the core inventions in the development of a TMP fiber analysis system for the MDF industry.

According to Wessbladh and Mohr [18], fiber suspension-based screen and image analysis techniques (Bauer-McNett, Shive Analyser, PQM) are presumed to be suitable for TMP characterization. However, these systems could not be established operationally as seen in a global survey on how fiber quality is determined in the MDF industry (cf. [5]). Besides the innovative (non-liquid) fiber pre-separation, and flow line tracing during image analysis, the successful software-based separation of cross-laying fibers can be seen as one of the core inventions in the development of a TMP fiber analysis system for the MDF industry.

Moreover, the system has proven to work stable by analyzing millions of fibers in thousands of images in a first industrial trial. Thus, it will be used in future as the first system to replace the haptical and visual analysis of experts by means of a laboratory system. In addition, the proposed algorithm outperforms other competitive approaches by using sub-pixel accuracy (cf. [19]). Despite other works on fiber recognition, this accuracy is needed due to the large range of fiber sizes, to ensure the accurate measurement of smallest fibers (cf. [2, 3]).

The experiments have shown that the proposed algorithm outperforms the formerly used software at the Thünen Institute of Wood Research by means of correctness of the measurements, the derivable parameters and the precision of each derived fiber property. In addition, the proposed algorithm outperforms other competitive approaches by using sub-pixel accuracy. The time needed for analyzing MDF fibers by mass image processing instead of manual microscopic measurements reduces from the order of years to minutes, without any loss in quality of the resulting statistics.

## 7 Acknowledgements

The authors are grateful to the Fachagentur Nachwachsende Rohstoffe e.V. (FNR) for funding the initial collaborative project "Fiber-Vision", in which the basic research could be performed. Further thanks are to the AiF Projekt GmbH for funding the successor project "Fiber-View". We would also like to thank Oliver Pieper, Erik Flick and Dennis Götsch as well as Wolfgang Bartz. They mainly influenced the development of the hardware and software components. Parts of the proposed setup have been patented.

## References

1. Bian, J., Qiu, S.: Pulp fibre recognition based on curvelet transform and skeleton tracing algorithm. In: Industrial Electronics and Applications, 2007. ICIEA 2007. 2nd IEEE Conference on. (2007) 2534–2538
2. Xu, B., Ting, Y.L.: Fiber-image Analysis Part I: Fiber-image Enhancement. Journal of the Textile Institute **87** (1996) 274–283
3. Xu, B., Ting, Y.L.: Fiber-image Analysis Part II: Measurement of General Geometric Properties of Fibers. Journal of the Textile Institute **87** (1996) 284–295
4. : FAO Yearbook of Forest Products 2010. Food and Agriculture Organization, Rome, Italy (2012)
5. Benthien, J.T., Ohlmeyer, M., Pieper, O., Heldner, S., Tackmann, O., Bähnisch, C., Hasener, J.: Determination of MDF fiber size distribution: Requirements and innovative solution. In: Proceedings of the International Wood Composites Symposium. (2013)
6. Benthien, J.T., Heldner, S., Seppke, B., Bähnisch, C., Ohlmeyer, M.: Innovativer ansatz zur bestimmung der faserlänge. Holz-Zentralblatt **41** (2014) 1000
7. Blum, H.: A transformation for extracting new descriptors of shape. In Wathen-Dunn, W., ed.: Proc. Models for the Perception of Speech and Visual Form, Cambridge, MA, MIT Press (1967) 362–380
8. Levi, G., Montanari, U.: A grey-weighted skeleton. Information and Control **17** (1970) 62 – 91
9. Gonzalez, R.C., Woods, R.E.: Digital Image Processing. 2nd edn. Addison-Wesley Longman Publishing Co., Inc., Boston, MA, USA (2001)
10. Choi, H.I., Choi, S.W., Moon, H.P.: Mathematical theory of medial axis transform. Pacific Journal of Mathematics **181** (1997) 57–88
11. Dimitrov, P., Phillips, C., Siddiqi, K.: Robust and efficient skeletal graphs. In: Proc. CVPR, Hilton Head, South Carolina (2000)
12. Steger, C.: Subpixel-precise extraction of lines and edges. In: International Archives of Photogrammetry and Remote Sensing. Volume XXXIII, part B3. (2000) 141–156
13. Köthe, U.: Reliable Low-level Image Analysis. PhD thesis, University of Hamburg (2007) Habilitation thesis.
14. Roerdink, J.B., Meijster, A.: The watershed transform: Definitions, algorithms and parallelization strategies. Fundam. Inf. **41** (2000) 187–228
15. Meine, H.: The GeoMap representation: on topologically correct sub-pixel image analysis. PhD thesis, University of Hamburg, Dept. Informatics (2009)
16. Köthe, U.: Generische Programmierung für die Bildverarbeitung. Books on Demand GmbH (2000)
17. Blanchette, J., Summerfield, M.: C++ GUI Programming with Qt 4. Prentice Hall PTR, Upper Saddle River, NJ, USA (2006)
18. Wessbladh, A., Mohr, R.: Faserfeinheiten: Moderne analysenethoden liefern online-qualitätsindizes [fiber fineness: Modern analysis methods deliver online quality indexes]. MDF-Magazin, DRW-Verlag Weinbrenner GmbH & Co, Leinfelden-Echterdingen, Germany (1999)
19. Wit, W., Köhler, U., List, J.: Hochgeschwindigkeits-bildanalyse zur charakterisierung von partikelgröße und -form. Produktgestaltung in der Partikeltechnologie **6** (2013) 213–239